Journal of Alloys and Compounds 502 (2010) 139–146

Contents lists available at ScienceDirect

Journal of Alloys and Compounds

journal homepage: www.elsevier.com/locate/jallcom

Serrated flow and work hardening characteristics of Al-5356 alloy

G. Saad [a], S.A. Fayek [b], A. Fawzy [a,*], H.N. Soliman [a], E. Nassr [a]

[a] Physics Dpt., Faculty of Education, Ain Shams University, Elmakrezy, Cairo 1174, Egypt
[b] Physics Dpt., National Center for Radiation Research and Technology, Nassr City, Cairo, Egypt

ARTICLE INFO

Article history:
Received 2 March 2010
Received in revised form 12 April 2010
Accepted 14 April 2010
Available online 22 April 2010

PACS:
62.20.Fe
61.82.Bg
61.66.Dk

Keywords:
Metals and alloys
Precipitation
Microstructure
X-ray diffraction
Serration

ABSTRACT

Stress–strain characteristics of Al-5356 are studied. Stress oscillation (repetitive stress drop or serration) in stress–strain relations (jerky flow or the Portevin–Le Chatelier (PLC)) was observed at the temperature ranging from 303 to 373 K at strain rate (S.R.) of 1.5×10^{-3} s^{-1}. A relation between the stress reload parameter $\Delta\sigma_R$ and the strain ε in the jerky flow was found to be in the form $[\Delta\sigma_R = A\exp(\varepsilon/\alpha)]$ with a growth constant α independent on grain diameter d and /or deformation temperature T_w. The effect of grain diameter d on the work-hardening parameters (WHP) yield stress σ_y, fracture stress σ_f, total strain ε_T, work-hardening coefficient $\chi_p(=d\sigma^2/d\varepsilon)$ and the strain-hardening exponent $n(=d\ln\sigma/d\ln\varepsilon)$ of Al-5356 alloy were evaluated at the applied deformation temperature range. The grain diameter d and deformation temperature T_w significantly decreased the total strain ε_T, the yield stress σ_y and the fracture stress σ_f of the tested samples, while the strain-hardening exponent n changed slightly. The relationship between the yield stress σ_y of the alloy under investigation and temperature follows an Arrhenius law. The mean activation energy of the deformation process was found to be ~87 kJ/mole, close to the activation energy of grain boundary diffusion in aluminum alloy.

1. Introduction

The high strength to weight ratio, high strength, good formability, excellent corrosion resistance and good weldability make aluminum alloys the preferred metals for many manufactured products such as automotive industry. This has greatly increased in recent years. In the last few decades, a series of active research has been made on the development of such lightweight metals, driven by the need to increase fuel efficiency, by making lightweight automobiles [1,2]. With increasing trend to substitute some automobile parts with light alloys, Al–Mg alloys combine corrosion resistance with reasonable strength, ductility and weldability. Therefore it has become of interest in lightweight structural applications in the transportation industry. Alloying elements are usually added to aluminum to increase its strength by two methods: (a) disperse alloying elements in solid solution and cold work the alloy (work-hardening alloys), and (b) dissolve the alloying elements into solid solution and precipitate them as coherent particles (precipitation-hardening alloys). Magnesium forms a solid solution in Al and it can be dissolved up to 10 wt.% at high temperatures [3]. Also, it is attractive as an alloying element since it is known to enhance the recovery process within Al, which may enhance super plastic response of this alloy.

Solder alloys serve as structural materials to sustain components. To ensure the reliability of solder joints, knowledge is required about the mechanical properties of the solder under service conditions. Furthermore, in order to analyze the stress or the strain distribution of solder joints subjected to mechanical or thermal loading, the stress–strain curves under various loading conditions should be determined.

During plastic flow, the spatial arrangement of dislocation ensembles derives from interactions of dislocations with strong and dense local obstacles other than dislocations (solute atoms, precipitates, lattice friction, Peierls forces, etc.) on the one hand, and on the other hand from their mutual interactions. If observed sufficiently large with a resolution scale, the former usually induces rather than uniform dislocation distributions and plastic flow, whereas the latter, which tends to prevail as deformation proceeds and dislocations multiply, leads to the emergence of collective behaviour and patterning [4]. Thus, at some stage uniform plastic flow may become unstable and may give way to localized straining. Then, the spontaneous formation of patterns, sometimes regular, sometimes propagating, may be observed on the surface of the deformed material. Jerky flow or the Portevin–Le Chatelier (PLC) effect is one of the most prominent examples of such plastic instabilities.

Three types of bands have been commonly distinguished in polycrystals in simple tension under constant applied strain rate

* Corresponding author. Tel.: +0020239770940; fax: +20 25428940.
E-mail address: afawzy1955@yahoo.com (A. Fawzy).

0925-8388/$ – see front matter © 2010 Elsevier B.V. All rights reserved.
doi:10.1016/j.jallcom.2010.04.119

Table 1
The chemical compositions of the Al-5356 solder alloy.

Al	Mg	Fe	Cu	Si	Mn	Cr	Zn	Ti	Be
93.5–94.5	4.5–5.5	0.4	0.1	0.25	0.05–0.2	0.05–0.2	0.1	0.06–0.2	0.0008

[5–7]. Type A bands are seen at large strain rates. They propagate continuously and are associated with weak undulations in the stress–strain curve. Type B "hopping bands" occur at lower strain rates. They are static bands formed sequentially ahead of one another, thus, they are giving an impression of propagation. The associated stress drops are larger and more regular than in type A. At even lower strain rates, type C bands are static, but they nucleate randomly along the sample, and produce marked serrations of large amplitude on the stress–strain curve.

The Portevin–Le Chatelier (PLC) effect is observed during plastic deformation of many alloys at a specific regime of temperature, strain and strain rate. At an imposed strain rate, the stress–strain curve develops serrations associated with repeated initiation and sometimes propagation of deformation bands [6,8,9]. It has first been explained by Cottrell [10], with the collective repeated breakaway and recapture of dislocations from their solute clouds of foreign atoms that the diffusion velocity of which is of the same order of magnitude as the dislocation velocity (viscous flow). It has to be noted that the Cottrell theory is based on bulk diffusion, whereas later on, theoretical and experimental investigations indicated the pipe diffusion mechanism, i.e. the solute diffusion along the dislocation lines, to be more relevant, in particular at moderate and lower temperatures [11–17]. This process is known as dynamic strain aging (DSA). More specifically, solute atoms diffuse to and age mobile dislocations during their temporary arrest at local obstacles [7]. This diffusive process is commonly considered the reason for PLC instabilities. This dynamic strain ageing can lead to a negative strain rate sensitivity of the flow stress within a certain range of applied strain rates and temperatures. This is when both types of defect have comparable mobility [11,18,19].

The present work is devoted to get an insight and provides some additional information about the effect of the grain diameter d on the (i) work-hardening parameters of Al-5356 specimens over a temperature range from 303 to 373 K and (ii) PLC phenomenon in Al-5356 solder alloy.

2. Experimental procedures

2.1. Sample preparation

This study has been carried out on commercial Al-5356 alloy supplied from Alumisr factory-Helwan-Cairo-Egypt in the form of rod of 3 mm in diameter. The chemical compositions of the solder alloy under investigation are given in Table 1. The rods were cold drawn in steps to wires 0.6 mm in diameter for stress–strain measurements. A part of the alloy was rolled into sheet of 0.3 mm in thickness and 5 mm width for microstructure investigation.

2.2. Heat treatment and structure examination

Samples in the form of sheet (5 mm × 6 mm) and wires (50 mm in length) of different grain diameters were obtained by annealing three groups of samples for 5 h in the solid solution region at the temperatures 673, 723 and 823 K, respectively using a thermo regulated furnace to produce stable grain sizes. The temperature inside the furnace was constant to within ±2 K. After annealing, the specimens were air quenched. Structure of the heat treated samples was examined by optical, scanning electron microscope (SEM), energy dispersive X-ray spectrometer (EDS) and X-ray diffraction (XRD) investigations. Prior to optical microscope examination, the samples were electropolished using an electrolyte consisted of 35% ortho-phosphoric, 40% ethanol and 25% water. To reveal the grain boundaries, the specimens were etched with 90% ortho-phosphoric acid. The average grain diameters obtained were 10, 14 and 23 μm, as determined optically by the line intercept method. Optical and SEM micrographs for specimens with different grain diameters, given in Figs. 1 and 2, showed that a dark phase decreased in size and seemed to be segregated at grain boundaries with the increase of the grain diameter.

EDS analysis (shown in Fig. 3) was performed on some heat treated samples of Al-5356 alloy. Different dark zones of Fig. 2a were selected for the detection of the elemental composition, the mean percentage of Al and Mg elements yielded the values of 96.4 and 3.6, respectively.

XRD investigations of these samples and analysis of the diffraction patterns were performed and a representative one corresponding to the grain diameter 10 μm is shown in Fig. 4. This figure showed that the obtained spectral lines correspond to (i) fcc Al matrix at (1 1 1) and (2 0 0), (ii) Mg at (1 0 4), (iii) β-phase (Al_3Mg_2) at (19 5 1) and (16 16 4), and (iv) $AlFe_3$ at (4 4 0) crystallographic planes at definite positions irrespective of the grain diameter. Only the relative intensities of these spectral lines were changed. As shown in Fig. 5, the decrease of the particle size associated with increasing the grain diameter is confirmed by calculating the particle size (t) from the half width of the spectral lines corresponding to Al_3Mg_2 phase using the formula [20]:

$$t = \frac{\lambda}{B\cos\theta} \quad (1)$$

where λ is the used wavelength in the X-ray diffraction patterns and B is the diffraction line measured at half its maximum intensity (radians).

3. Experimental results and observations

Experimental sets of stress–strain relations were performed at different temperatures for the alloy wires having different grain diameter by using a tensile testing machine described elsewhere [21]. The deformation temperature studied 303, 323, 348 and 373 K. The wires were heated while they were clamped in the tensile testing machine. The strain rate was kept constant at $1.5 \times 10^{-3}\ s^{-1}$ in all experiments.

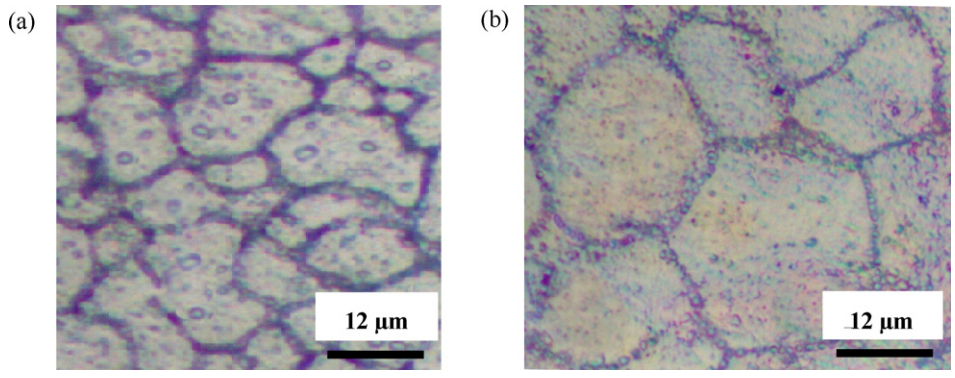

Fig. 1. Photomicrographs of Al-5356 alloy specimens annealed for 5 h at (a) 673 K (10 μm) and (b) 823 K (23 μm).

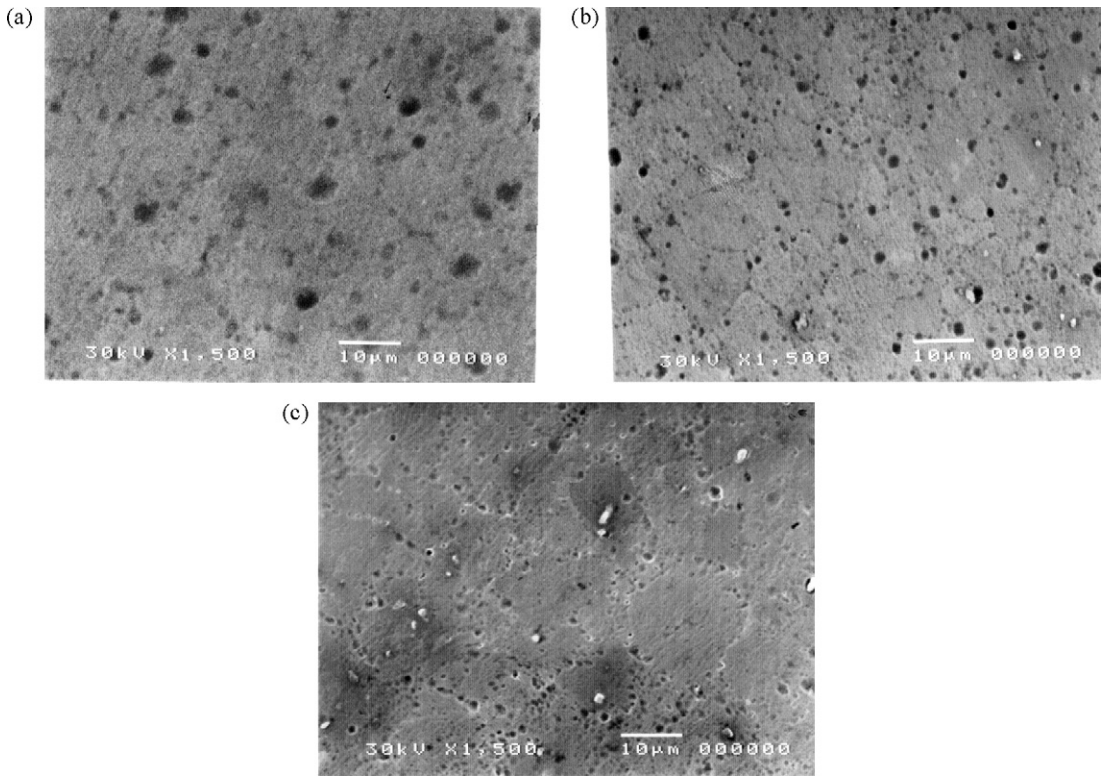

Fig. 2. Scanning electromicrographs of Al-5356 alloy specimens annealed for 5 h at (a) 673 K (10 μm), (b) 773 K (14 μm), and (c) 823 K (23 μm).

3.1. Effect of grain diameter and deformation temperature

Fig. 6 represents a set of stress–strain curves for the three grain diameters carried out at room temperature. Similar curves were obtained at deformation temperatures (323, 348 and 373 K). From Fig. 6 it is clear that:

(i) Stress–strain curve of the smaller grain diameter is shifted higher than the larger ones, which mean higher work-hardening parameters namely, fracture stress σ_f, yield stress σ_y, total strain ε_T and work-hardening coefficient χ_p.
(ii) A serration behaviour is observed in all the stress–strain curves in all different grain diameters.
(iii) The difference between the upper and lower limits of the serration (serration amplitude) was found to be inversely proportional to the grain diameter i.e., the larger the grain diameter is, the smaller the serration amplitude becomes which means the weaker serration process.

3.2. The work-hardening parameters

From the representative stress–strain curves of Fig. 6 and similar curves at different deformation temperatures, it was clear that increasing the deformation temperature decreased both the yield stress σ_y and fracture stress σ_f. For wires tested at different deformation temperatures, an inverse relation was found between σ_f and grain diameter d. This relation is linear as shown in Fig. 7a. Extrapolation of these lines intersects at a point of unique grain diameter that makes the value of σ_f independent on deformation temperature. The relation between the yield stress σ_y and grain diameter was also found similar to that obtained with σ_f as shown in Fig. 7b. The unique grain diameter for both σ_f and σ_y was found to be ~29 μm at which σ_f and σ_y correspond to the values 90 and 38 MPa, respectively. This confirms the decrease of both σ_f and σ_y with increasing d.

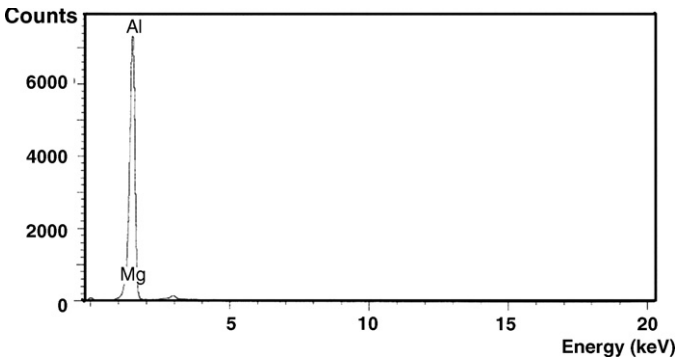

Fig. 3. EDS for the Al-5356 alloy showing the existence of Al and Mg elements.

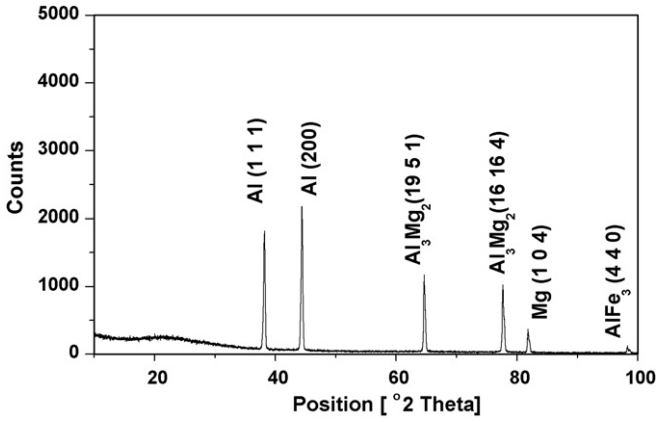

Fig. 4. X-ray diffraction pattern of the Al-5356 alloy under investigation.

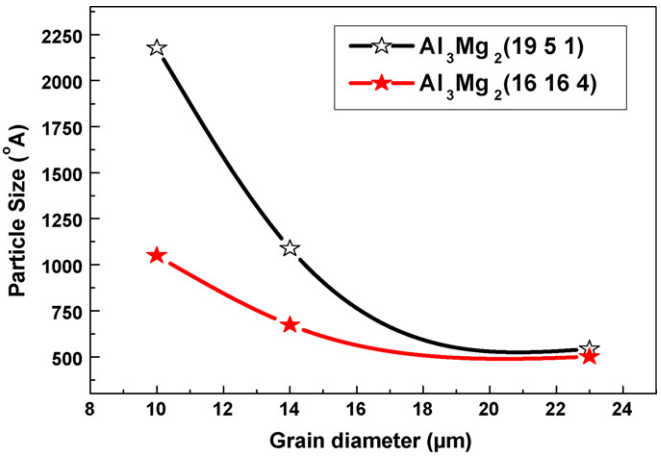

Fig. 5. The grain diameter dependence of particle size in the Al-5356 alloy.

The temperature dependence of the total strain ε_T is shown in Fig. 8 which indicates that, the total strain ε_T decreased at any given deformation temperature with increasing grain diameter d. While at any given grain diameter, it decreased with increasing the deformation temperature T_w until it reached a minimum value at 348 K, and then increased with increasing T_w.

Above a strain of 0.002 ($\varepsilon > 0.002$), the stress–strain curves were parabolic around the yield stress σ_y. Accordingly, the work-hardening coefficient $\chi_p (=d\sigma^2/d\varepsilon)$ [22] was calculated. Fig. 9 shows a representative linear relation between σ^2 and ε for specimens with different grain diameters tested at 303 K. The work-hardening coefficient χ_p was calculated from the slopes of these straight lines and the grain diameter dependence of it is shown in Fig. 10. From this figure, it is clear that the work-hardening coefficient χ_p decreases with increasing both the grain diameter and deformation temperature.

3.3. Strain-hardening exponent

At strain >0.002, the stress–strain curves were found to obey the well-known power law [23]:

$$\sigma = \beta\varepsilon^n \tag{2}$$

where β is the strength coefficient and n is the strain-hardening exponent. Fig. 11 shows a representative linear relation between $\ln\sigma$ and $\ln\varepsilon$ for specimens with different grain diameters tested at 303 K. Values of n were calculated from the slopes of these straight lines at the different deformation temperatures as illustrated in Fig. 12. It is clear that n decreases slightly with the increase of both the grain diameter d and the deformation temperature T_w.

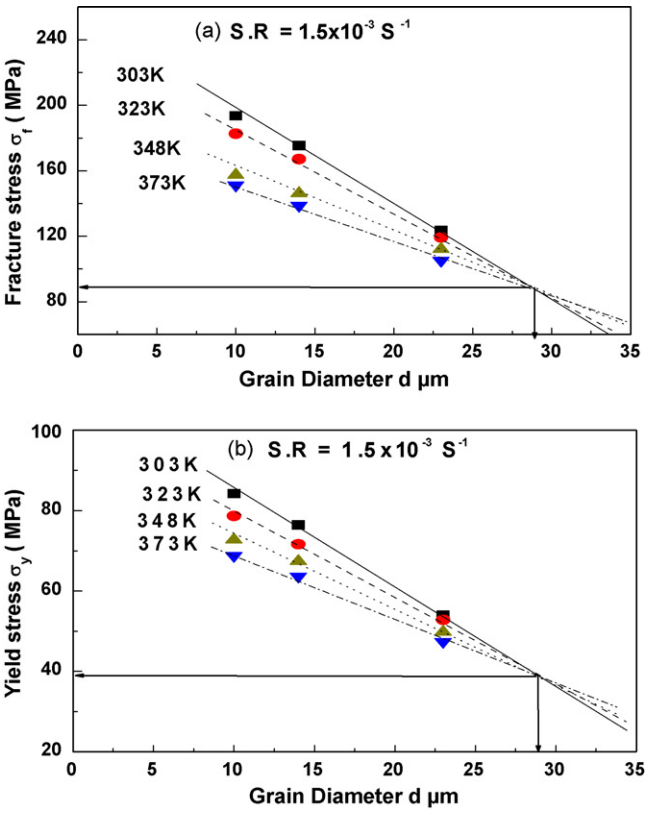

Fig. 7. Dependence of the work-hardening parameters on d for (a) the fracture stress σ_f, and (b) the yield stress σ_y for specimens tested at different deformation temperatures.

3.4. The activation energy (Q)

The energy activating the deformation process may be evaluated from the variation of the yield stress σ_y, as related to the deformation temperature T_w, through the kinetic rate equation [21]:

$$\sigma_y = k\left[\dot{\varepsilon}\exp\left(\frac{Q}{RT}\right)\right]^m \tag{3}$$

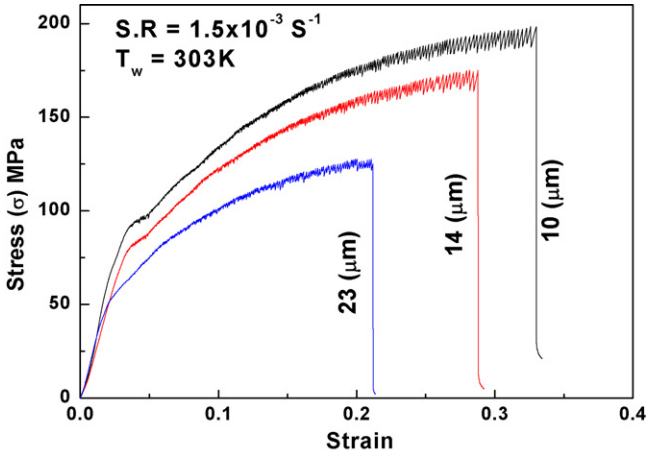

Fig. 6. Representative stress–strain curves of Al-5356 specimens at different grain diameters (10, 14 and 23 μm) and tested at 303 K.

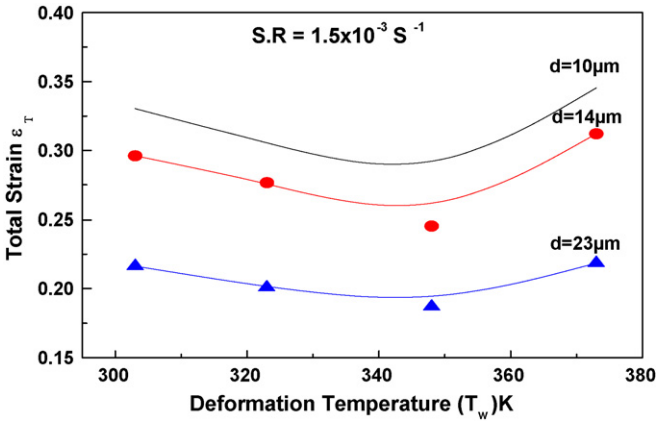

Fig. 8. The deformation temperature dependence of the total strain ε_T for Al-5356 alloy specimens having different grain diameters.

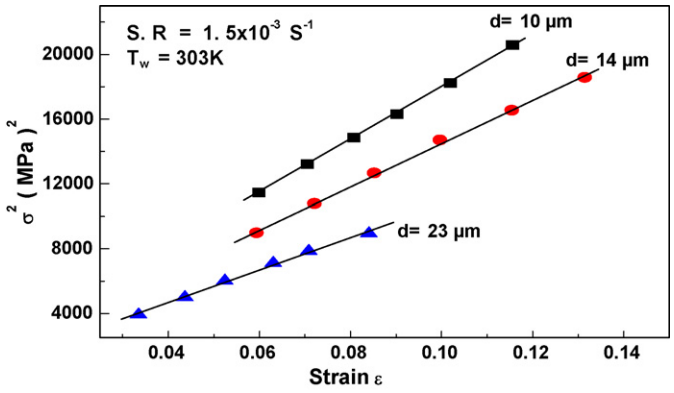

Fig. 9. Representative relation between σ^2 vs. ε for Al-5356 alloy specimens tested at 303 K with different grain diameters.

where k is a material constant, $\dot{\varepsilon}$ is the strain rate, R is the universal gas constant and m is the strain rate sensitivity index. To estimate the value of the activation energy Q for the deformation process, the standard Arrhenius plot of $\ln \sigma_y$ vs. $1000/T$ is to be constructed as shown in Fig. 13. From the slopes of the obtained straight lines, the calculated mean value of the activation energy Q was found 87 kJ/mole, which is in accordance with that obtained in similar work by Yong-yi et al. [24].

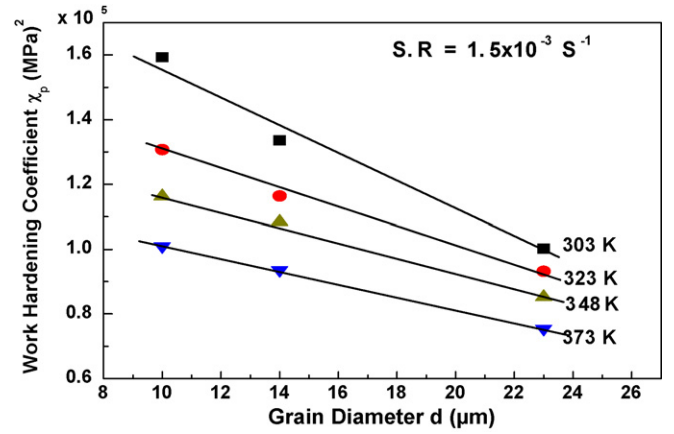

Fig. 10. Grain diameter dependence of the work-hardening coefficient χ_p for Al-5356 alloy specimens tested at different deformation temperatures.

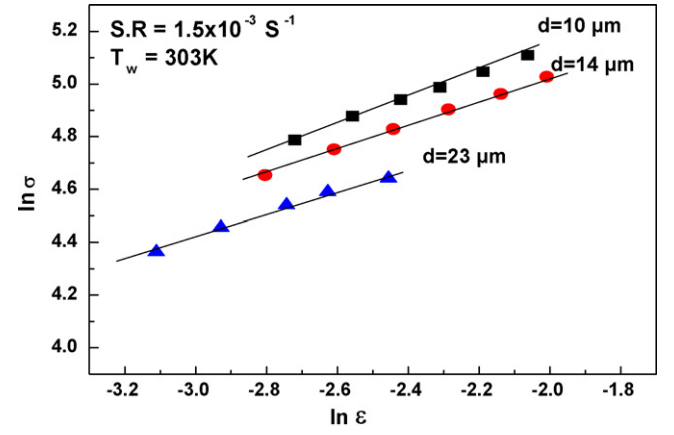

Fig. 11. Representative relation between $\ln \sigma$ vs. $\ln \varepsilon$ for Al-5356 alloy specimens tested at 303 K having different grain diameters.

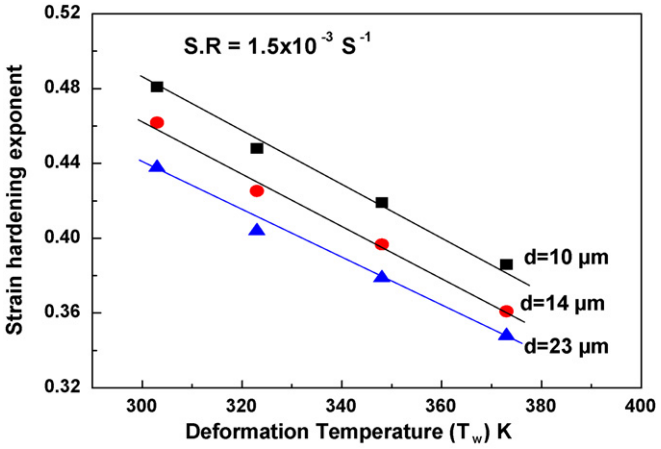

Fig. 12. Temperature dependence of the strain-hardening exponent n.

3.5. The serration characteristics

In the present study on Al-5356 alloy, a stress oscillation (stress drop or serration) in stress–strain relations (jerky flow or the Portevin–Le Chatelier (PLC)) was observed at the temperature ranging from 303 to 373 K at strain rate of 1.5×10^{-3} s^{-1}. From Fig. 6, it is clear that in the plastic deformation region, the stress amplitude $\Delta\sigma$ is found to (i) increase with increasing strain at any grain diameter and (ii) decrease with increasing the grain diameter d.

It was reported earlier that an electronic noise – similar to actual serrations – is superimposed on the signals from the load cell [25]. Software has now been developed to minimize these aberrations in the load-extension curve. One way to smooth the curve is by averaging a few successive data points and plotting only such average values. It was found that averaging ten successive data points minimizes the scatter due to the noise without altering the true response from the sample. To get more characteristics of the serrated part in the stress–strain curve, it was convenient to magnify this part and construct a relation between stress and time as shown in Fig. 14, thus the following parameters can be identified [26]:

(i) The stress reload $\Delta\sigma_R$, which is the stress difference between the beginning and the end of the serration step in the reloading range.
(ii) The reloading time Δt_R, which is the time needed for the reloading process.
(iii) The stress drop $\Delta\sigma_D$, which is the stress difference between the highest and lowest points of a serration step.

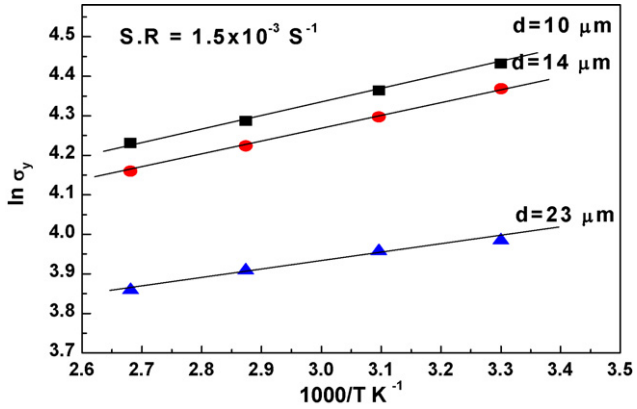

Fig. 13. Arrhenius plot of $\ln \sigma_y$ vs. $1000/T$ for Al-5356 alloy.

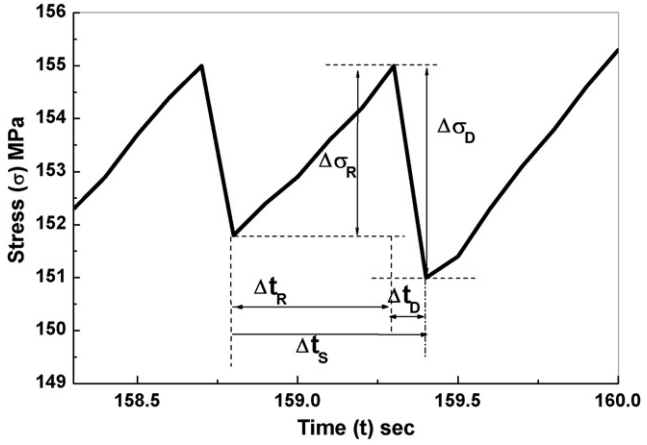

Fig. 14. An enlarged portion of a computer-recorded stress–time curve with various parameters defined.

(iv) The drop time Δt_D, which is the time elapsed during a stress drop.
(v) The period of a serration Δt_S; this is the time interval between the onsets of two successive serration steps.

For each serration step, the serration parameters were calculated for each grain diameter at all applied deformation temperatures. The dependence of the size of the stress reload value $\Delta\sigma_R$, as a representative serration parameter, on the plastic strain which is obtained from an automated evaluation, is plotted in Fig. 15a. Since serrations along a stress–strain curve are rarely completely uniform, the data of the stress reloads scatter widely. It was found that the stress reload $\Delta\sigma_R$ increases exponentially with the

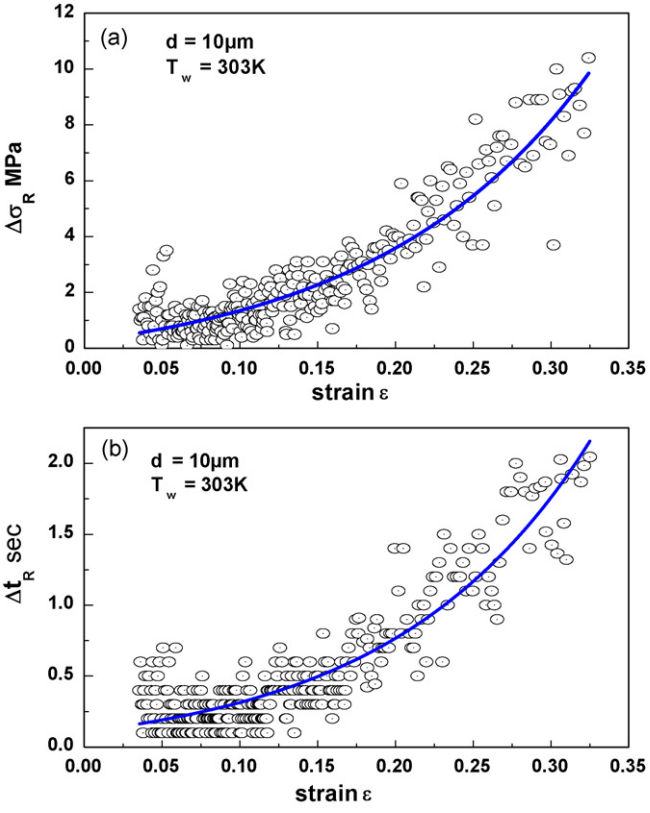

Fig. 15. The dependence of (a) the stress reloads $\Delta\sigma_R$ and (b) the time reloads Δt_R on plastic strain.

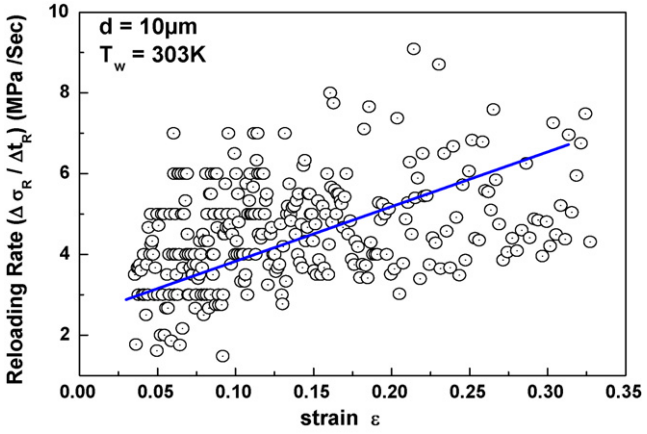

Fig. 16. Reloading rate as a function of strain.

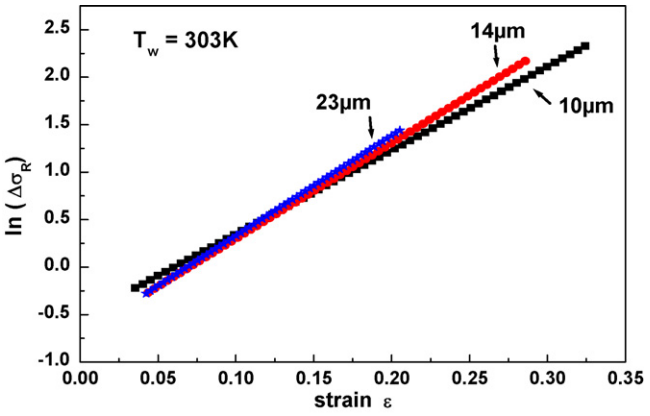

Fig. 17. Representative relation between $\ln(\Delta\sigma_R)$ vs. ε for Al-5356 alloy specimens tested at 303 K with different grain diameters indicated in the figure.

plastic strain for all different grain diameters and deformation temperatures. The best fit exponential behaviour was found to obey the equation:

$$\Delta\sigma_R = A\exp\left(\frac{\varepsilon}{\alpha}\right) \quad (4)$$

where A is a constant and α is the serration growth constant. The dependence of the reloading time Δt_R on the plastic strain was also found similar to that obtained with $\Delta\sigma_R$ as shown in Fig. 15b. Moreover, the reloading rate $\Delta\sigma_R/\Delta t_R$ is increased with strain as seen in Fig. 16 and it can be concluded that the time for segregation of solute atoms at the dislocation line increases as the load rate decreases.

A representative linear relation between $\ln(\Delta\sigma_R)$ and ε for specimens tested at 303 K for the grain diameters 10, 14 and 23 μm is shown in Fig. 17. Straight lines were obtained, the slope of which gave the values of $(1/\alpha)$. The calculated values of α were found to be 0.111, 0.109 and 0.099 for the grain diameters 10, 14 and 23 μm, respectively. These results indicated that the growth constant α is independent on the grain diameter of the tested samples. Similar calculation at the different deformation temperatures indicated that α is also independent on the deformation temperature.

4. Discussion

Concerning the structure of the heat treated samples under investigation, the morphology was observed in the SEM and the dark phase was examined with the energy dispersive X-ray spectrometer (EDS) (see Fig. 3). The investigation by XRD showed the

existence of the β-phase intermetallic compound Al_3Mg_2, as illustrated in the diffraction pattern of Fig. 4. According to what is mentioned before, the general feature of the obtained stress–strain curves was found to be sensitive to both the grain diameter d and the deformation temperature T_w exhibiting repetitive stress drops in the stress–strain curves. It is clear from Fig. 2 that increasing the grain diameter was associated with a refinement in the particle size. This refinement may be a result of increasing the annealing temperature to about $0.72–0.9T_m$ to achieve larger grain diameters, which may result in partial dissolution of larger β-phase particles and coalesce of ultra fine ones. The refinement may result in the decrease of the height of the obstacles to dislocation motion, thus, the decrease of the work-hardening parameters σ_f and σ_y can be accounted for. It should be noted that as the particle size decreases, while raising the annealing temperature to increase the grain diameter, a process of migration of these particles takes place towards the grain boundaries as seen in Figs. 1b and 2b, c. Consequently, the surface energy of the boundaries becomes higher; therefore low stress is needed for intergranular fracture to take place. Thus, the observed low total strain ε_T with increasing the grain diameter can be explained.

The unique value of d (∼29 μm) obtained in Fig. 7a and b means that the fracture becomes athermal process for this grain size and the stress required to attain the fracture is $\sigma_f \sim 90$ MPa. In addition, the maximum stress, which still maintains the material within the elastic region, is $\sigma_y \sim 38$ MPa without thermal agitation.

Regarding the effect of deformation temperature, it is known that the hardenability of a polycrystalline material is reduced by raising the deformation temperature [27]. This recovery reaction is responsible for the observed decrease in wires hardenability as measured by σ_f and σ_y (Fig. 7a and b) this is from one hand. On the other hand the decrease in the total strain ε_T (Fig. 8) at deformation temperature less than 348 K is due to pinning of dislocations that cannot breakaway from these pinning centers. While at temperatures higher than 348 K, breakaway process takes place and dislocations can move freely leading to an increase in the total strain ε_T.

As the investigated samples showed parabolic hardening characteristics, it is acceptable to adopt Mott's [28] work-hardening model. This model predicts the relation for the coefficient of work-hardening

$$\chi_p = \frac{G^2 b}{2\pi^2 L} \tag{5}$$

where L is the distance slipped by moving dislocation, G is the shear modulus, and b is the interatomic distance. In the polycrystalline metals, grain boundaries limit the slip distance of dislocations from any source within grain. Accordingly, a small value of L leads to rapid hardening rate and vice versa on the one hand, this is consistent with the inverse relation between χ_p and the grain diameter shown in Fig. 10. On the other hand the decrease in the work-hardening coefficient χ_p with increasing the deformation temperature could be explained as due to the fact that when thermal agitation is increased, it is then easier for dislocation to overcome obstacles in the matrix. Thus the average slip distance L, will be increased [29], which gives rise to the decrease of χ_p.

It is well known that both the total strain ε_T and the strain-hardening exponent n of Eq. (2) are important factors in judging the formability of the material [23]. The large value of n means greater resistance to necking and is more suitable for forming options involving tensile deformation (more ductile). In other words, one fact of ductility is the ability to elongate without fracture [30]. From the variation of both ε_T and n with the grain diameter d, as seen in Figs. 8 and 12, it is clear that n showed similar behaviour of ε_T with d. Thus, the variation of the strain-hardening exponent n with d suggests that the mechanical response in this behaviour seems to be essentially affected by the accompanied variations of the internal structure of the tested material as has been discussed before.

The value of the energy activating the deformation process Q, calculated from Fig. 13, was found to be ∼87 kJ/mole, which is in accordance with that needed for the activation energy of grain boundary diffusion in aluminum alloy. It is found in agreement with the results obtained in other works [24,31–33].

Serrations, seem to be type B, observed in the obtained stress–strain curves in this work can be attributed to the presence of some retained Mg, Cu, and Si atoms in the solid solution treated samples besides β (Al_3Mg_2) and $AlFe_3$ phases. This is according to what has been detected from X-ray diffraction analysis. These entities may cause an anchoring of the dislocations created during the plastic deformation. A detachment of these dislocations requires instantaneous increase in stress (during tensile tests) in order to liberate the dislocations from the above mentioned phases. The observed decrease in stress, up to the moment of dislocation movement, is occurring at the subsequent defects. This is repeated periodically and serrations are attained in each stress–strain curve. As mentioned before in our experimental results, the serration amplitude ($\Delta\sigma$) was found to be inversely proportional to the grain diameter of the tested sample (see Fig. 6). This may be explained as follows: as the grain diameter increases, the particle size of the β-phase (Al_3Mg_2) decreases as shown in Figs. 2 and 5. Thus, the decrease of the serration amplitude with increasing the grain diameter can be accounted for. This is in agreement with the results obtained by Darowicki et al. [34].

5. Conclusions

The main conclusions to be drawn from this study may be summarized as follows:

(i) The WHP σ_f and σ_y decreased with increasing grain diameter and/or deformation temperature. The former was attributed to the refinement in the particle size, while the later makes thermal agitation more effective.
(ii) The total strain ε_T decreased with increasing the grain diameter, which might be attributed to the migration of the β-phase towards the grain boundaries leading to earlier fracture.
(iii) The total strain ε_T decreased with increasing the deformation temperature up to 348 K due to pinning of dislocations that cannot breakaway from these pinning centers. At temperatures higher than 348 K, a breakaway process takes place and dislocations can move freely leading to an increase in the total strain ε_T.
(iv) The work-hardening coefficient χ_p was found to be decreased with increasing grain diameter and/or deformation temperature. This is due to the decrease of the slip distance of dislocations.
(v) The mean value of 87 kJ/mole for the energy activating the deformation process is found to correspond with the activation energy of grain boundary diffusion in aluminum alloy.
(vi) The observed serration behaviour might be attributed to the presence of entities, which cause an anchoring of the dislocations leading to increase the stress necessary to liberate the dislocations from it. Then a decrease in stress takes place.
(vii) The growth constant α (∼0.1) in the serration equation $\Delta\sigma_R = A\exp(\varepsilon/\alpha)$ is found to be independent on both grain diameter and deformation temperature of the tested samples.

References

[1] T.R. McNelley, A.A. Salama, P.N. Kaln, Advances in Superplasticity and Superplastic Forming, TMS, Warrendale, PA, 1993, p. 45.

[2] B.S. Chung, D.Y. Maeng, S.I. Hong, Third Pacific Rim International Conference on Advanced Materials and Processing, 1998, p. 1879.
[3] D.Y. Maeng, J.H. Lee, S.I. Hong, Mater. Sci. Eng. A 357 (2003) 188–195.
[4] L.P. Kubin, C. Fressengeas, G. Ananthakrishna, in: F.R.N. Nabarro, M.S. Duesbery (Eds.), Dislocations in Solids, vol. 11, Elsevier Science BV, Amsterdam, 2002, pp. 101–192.
[5] S. Kok, M.S. Bharathi, A.J. Beaudoin, C. Fressengeas, G. Ananthakrishna, L.P. Kubin, M. Lebyodkin, Acta Mater. 51 (2003) 3651–3662.
[6] H. Ait-Amokhtar, S. Boudrahem, C. Fressengeas, Scripta Mater. 54 (2006) 2113–2118.
[7] H. Ait-Amokhtar, P. Vacher, S. Boudrahem, Acta Mater. 54 (2006) 4365–4371.
[8] R. Shabadi, S. Kumar, H.J. Roven, E.S. Dwarakadasa, Mater. Sci. Eng. A 364 (2004) 140–150.
[9] K. Chihab, H. Ait-Amokhtar, K. Bouabdellah, Ann. Chim. Sci. Mater. 27 (2002) 69.
[10] F.B. Klose, A. Ziegenbein, F. Hagemanna, H. Neuhäuser, P. Hähner, M. Abbadi, A. Zeghloul, Mater. Sci. Eng. A 369 (2004) 76–81.
[11] C.P. Ling, P.G. McCormick, Acta Metall. Mater. 41 (1993) 3127–3131.
[12] P.W. Balluffi, A.V. Granato, in: F. Nabarro (Ed.), Dislocations in Solids, vol. 4, North Holland Physics Publishing, Amsterdam, Oxford, New York, Tokyo, 1979, pp. 1–113 (Chapter 13).
[13] J. Schlipf, Scripta Metall. Mater. 29 (1993) 287–292.
[14] J. Schlipf, Scripta Metall. Mater. 31 (1994) 909–914.
[15] S.Y. Lee, Ph.D. Thesis, RWTH Aachen, 1993.
[16] F. Springer, Ch. Schwink, Scripta Metall. Mater. 25 (1991) 2739–2744.
[17] F. Springer, A. Nortmann, Ch. Schwink, Phys. Stat. Sol. A 170 (1998) 63–81.
[18] H. Ait-Amokhtar, C. Fressengeas, S. Boudrahem, Mater. Sci. Eng. A 488 (2008) 540–546.
[19] K. Chihab, C. Fressengeas, Mater. Sci. Eng. A 356 (2003) 102–107.
[20] B.D. Cullity, Elements of X-ray Diffraction, second edition, Addison-Wesley Publishing Company, Inc., 1978, p. 284.
[21] G. Saad, S.A. Fayek, A. Fawzy, H.N. Soliman, Gh. Mohammed, Mater. Sci. Eng. A 527 (2010) 904–910.
[22] N.F. Mott, Trans. Metall. Soc. AIME 218 (1960) 6.
[23] E. Diter George, Mechanical Metallurgy, SI Metric edition, McGraw-Hill Book Company, UK, 1988, p. 287.
[24] P. Yong-yi, Y. Zhi-min, N. Bo, Z. Li, Trans. Nonferrous Met. Soc. China 17 (2007) 744–750.
[25] H. Weinhandl, F. Mitter, W. Bernt, S. Kumar, E. Pink, Ser. Metall. Mater. 31 (1994) 1567.
[26] S. Kumar, H. Weinhandl, E. Pink, Mater. Sci. Eng. A212 (1996) 213–221.
[27] T.H. Youssef, G. Saad, Philos. Mag. A 42 (2) (1980) 217.
[28] N.F. Mott, Dislocation and Mechanical Properties of Crystals, Wiley, New York, 1957.
[29] M. Koiwa, R.R. Hastiguti, Trans. Jpn. Inst. Metals 81 (1976) 75.
[30] A. Fawzy, R.H. Nada, Physica B 371 (2006) 5.
[31] S.W. Lee, J.W. Yeh, Mater. Sci. Eng. A A460 (2007) 409–419.
[32] C.H. Manish, I. Roy, A.M. Farghalli, Mater. Sci. Eng. A A410 (2005) 24–27.
[33] D.H. Bae, A.K. Ghosh, Acta Mater. 48 (2000) 1207–1224.
[34] K. Darowicki, J. Orlikowski, A. Zielinski, W. Jurczak, Comput. Mater. Sci. 39 (2007) 880.